Supporting Information

Regulating Buried Interface Properties and Alleviating Micro-strain of Crystal for Efficient Perovskite solar cells

Shendong Xu,‡[ab] Guozhen Liu,‡*[a] Haiying Zheng,[c] Yuli Tao,[ab] Hui Zhang,[ac] Liying Zhang,[ab] Liangzheng Zhu,[ab] Jiajiu Ye,[a] Jinfeng Li*[d] and Xu Pan*[a]

[a]Key Laboratory of Photovoltaic and Energy Conservation Materials, Institute of Solid State Physics, Hefei Institutes of Physical Science, Chinese Academy of Sciences, Hefei 230031, P. R. China.

[b]University of Science and Technology of China, Hefei 230026, P. R. China.

[c]Institutes of Physical Science and Information Technology, Anhui University, Hefei, Anhui, 230601, P. R. China.

[d]Institute of Systems Engineering, Chinese People's Liberation Army Academy of Military Sciences, Beijing 100141, P.R. China.

*Corresponding author. E-mail: xpan@rntek.cas.cn

Experimental Section

Materials

The ammonium hexafluorophosphate (AHFP) were purchased from aladdin. The SnO_2 colloid precursor (tin (IV) oxide, 15% in H_2O colloidal dispersion) was obtained from Alfa Aesar. Methylammonium iodide (MAI), formamidinium iodide (FAI), methylammonium bromine (MABr), methylamine Chloride (MACl) and Spiro-MeOTAD (99.86%) both purchased from Xi'an Polymer Light Technology manufacturers. The lead (II) iodide (PbI_2), lead (II) bromide ($PbBr_2$) and cesium iodide (CsI) were purchased from TCI. DMSO (dimethylsulfoxide 99.50%), DMF (N,N-dimethylformamide 99.99%), chlorobenzene and isopropanol (IPA) from Sinopharm. Other materials have been acquired from Sinopharm or Alfa or Aldrich and all the commercial materials were used as received without additional treatment.

Perovskite Solar Cells (PSCs) Fabrication

A perovskite solar cell with structure "ITO/SnO_2/perovskite/ spiro-MeOTAD/Au" was prepared by one step method. The specific steps are as follows: Firstly, the etched ITO glass (1.5 cm × 2 cm) was cleaned by using the detergent for 15 min, ultrapure water for 20 min, and ethanol for 20 min, sequentially. And then, the etched ITO was treated through an ultraviolet ozone (UVO) for 30 min. The SnO_2 films were prepared by spin-coating the above SnO_2 colloidal solution (100 μL) on the etched ITO substrates at 4000 rpm for 50 s and then the SnO_2 films was annealed at 100 ℃ for 90 min. Afterwards, all the SnO_2 films were exposed to UVO for 30 min. And then, we spin-coated the AHFP-ethanol solution with different concentrations on the

SnO_2 underlying layer, followed by reannealing at 90 °C for 20 minutes. Afterwards, all SnO_2 films were exposed to UVO for 30min before setting aside.

The Pb^{2+} precursor solutions of $(FAPbI_3)_{0.925}(MAPbBr_3)_{0.05}(CsPbI_3)_{0.025}$ was fabricated by dissolving the corresponding amount of MAI, FAI, MABr, MACI, PbI_2, PbBr, CsI powders in anhydrous N,N-dimethylformamide (DMF) and dimethyl sulfoxide (DMSO) mixed solvent (DMF:DMSO = 4:1) with stirring at 25 °C for 50 min. The perovskite layers were coated by spin coating 1.6 M perovskite precursor solutions in dry air (humidity was kept at about 5% RH) flowing glovebox. Chlorobenzene (100 μL) was dropwise added on the substrate during the spin-coating step 15s before the end of the total procedures. The substrate was sintered at 150 °C for 15 min on a hotplate.

Subsequently, the hole-transporting material (HTM) solution was deposited on the perovskite layer by spin coating which was comprised of spiro-OMeTAD (73.5mg), 4-tert-butylpyridine, cobalt(III) salt and lithium bis-(trifluoromethanesulfonyl)imide and in chlorobenzene solvent.

Finally, the films were dried under vacuum before completing the device fabrication process by thermal evaporating 80 nm of Au on top of the HTM layer.

Characterization

PCEs and *J-V* curves were obtained via using a solar simulator (Newport, Oriel Class A, 91195A) and a source meter (Keithley 2420). SEM images were performed on a field-emission scanning electron microscope (Gemini SEM 500, Zeiss, Germany) with high-resolution. The Ultraviolet–visible absorption spectra were obtained from

ultraviolet-vis (UV-vis) spectrophotometer (U-3900H, HITACHI, Japan). Steady-state PL spectra were obtained from a spectrofluorometer (photon technology international). The exciting wavelength was 475 nm and excited by a standard 450 W xenon CW lamp and analyzed by the software Fluorescence. The time-resolved PL experiments were performed with the same Fluorescence Lifetime Spectrofluorometer using a pulsed source at 450 nm (the illumination source is a pulsed nitrogen dye laser) and the signal was recorded at 770 nm by the Time Correlated Single Photon Counting (TCSPC) technique. X-ray photoelectron spectra (XPS) and Ultraviolet photoelectron spectra (UPS) measurements were collected with Thermo ESCALAB 250Xi system. Depth-dependent grazing incident X-ray diffraction (GIXRD) patterns with 2θ range from 0.3° to 1.5° (step 0.2°) were carried out on a Small Angle X-ray scatterer (SAXSpoint2.0). X-ray diffraction (XRD) patterns with 2θ range from 5° to 70° were carried out on a Rigaku smartlab 9KW with Cu Kα radiation. Contact angles were conducted on an OCA15EC contact angle measuring instrument (Dataphysics, Germany) with a drop of ultrapure water. EIS at 0.6 V was tested on an Autolab analyzer(Metrohm, PGSTAT 302N, Switzerland) in the dark with a frequency range from 0.1 Hz to 1 MHz. IPCE with a wavelength range from 300 to 900 nm were tested with dual Xenon/quartz halogen light source (PV Measurements, Inc.), and measured in DC mode with no bias light used. The solar simulator with 100 mW/cm^2 illumination AM 1.5G was calibrated via a Si-reference cell which was certified by NREL. Via masking a black mask, the devices retained an active area of 0.09 cm^2.

DFT calculations of the formation energy

The formation energy of iodine vacancy defects in un-adsorbed and adsorbed conditions is used to illustrate the calculation method and process. Firstly, the defect formation energy is calculated according to the following formula: E (defect formation energy) = E (perovskite structure containing iodine defect) -E (structure without I defect) + (1/2) E (I_2); Respectively represent the formation energy of iodine vacancy defect, the total energy of a system containing one iodine vacancy defect, the total energy of a system without iodine vacancy defect, and the total energy of I_2. Based on this, we calculated the corresponding defect formation energy after replacing an iodine atom on the surface of the crystal with PF_6^-ion.

The whole calculation is based on the VASP platform, and its specific parameters and boundary conditions are set according to the previously reported articles.[1-3]

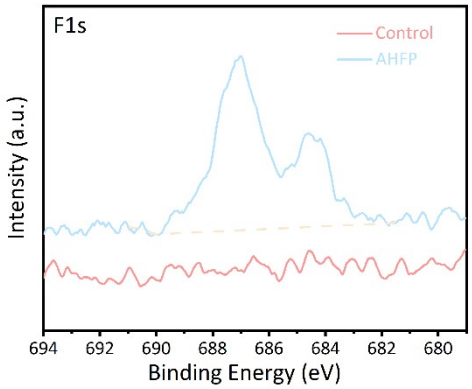

Fig. S1 XPS spectra of control and AHFP-treated SnO_2 films for F1s.

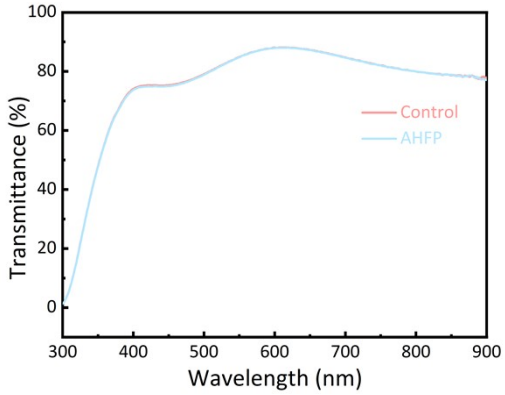

Fig. S2 Optical transmittance spectra of control and AHFP-treated SnO_2 films.

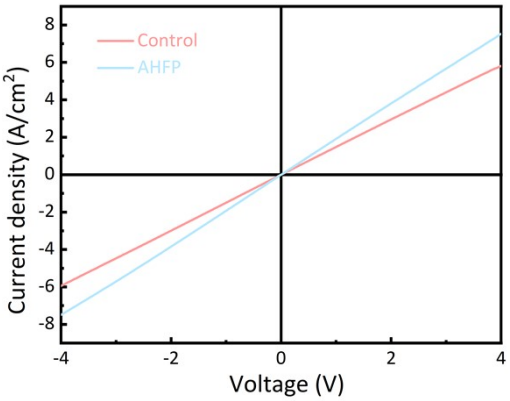

Fig. S3 $J-V$ characteristics of device with the architecture of ITO/SnO_2/Au and ITO/SnO_2-AHFP/Au.

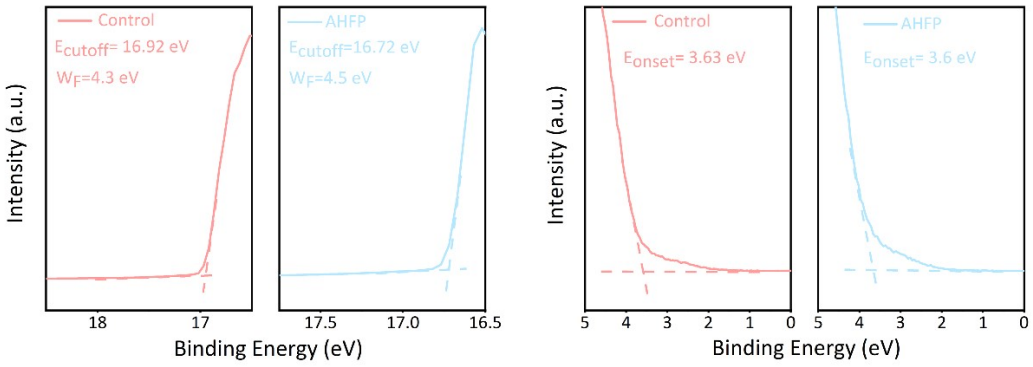

Fig. S4 UPS spectra of control and AHFP-treated SnO_2 films.

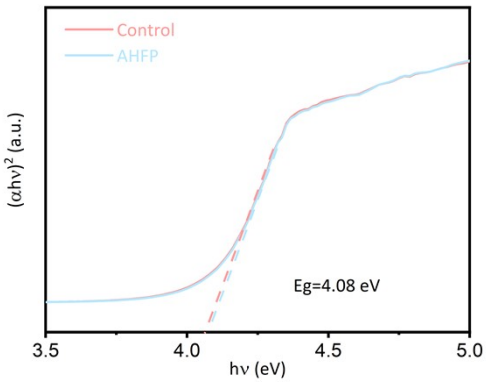

Fig. S5 $(\alpha h\nu)^{1/2}$ as a function of photon energy from Ultraviolet–visible absorption spectra.

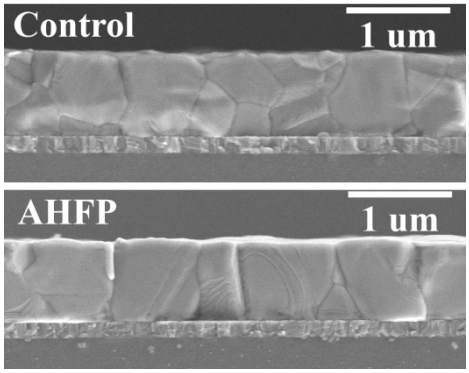

Fig. S6 The cross-sectional SEM images of perovskite films on the control and AHFP-treated SnO_2 films.

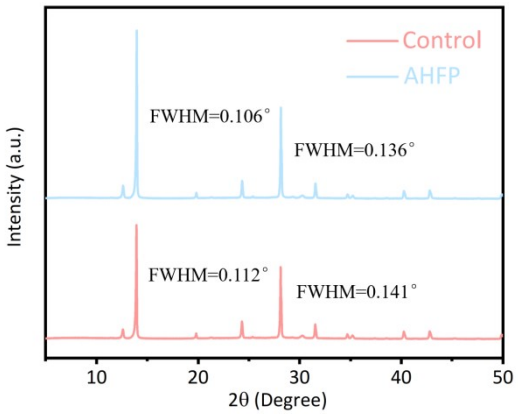

Fig. S7 XRD patterns of perovskite films on the control and AHFP-treated SnO_2 films.

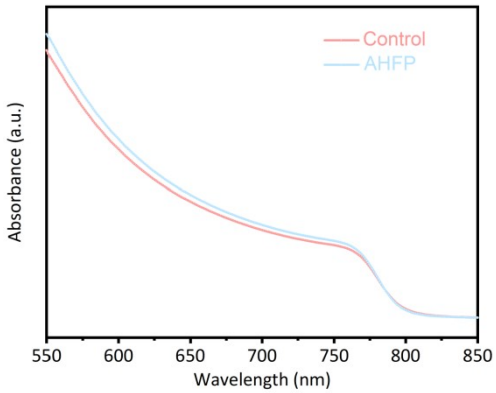

Fig. S8 UV-vis absorption spectra of perovskite films on the control and AHFP-treated SnO_2 films.

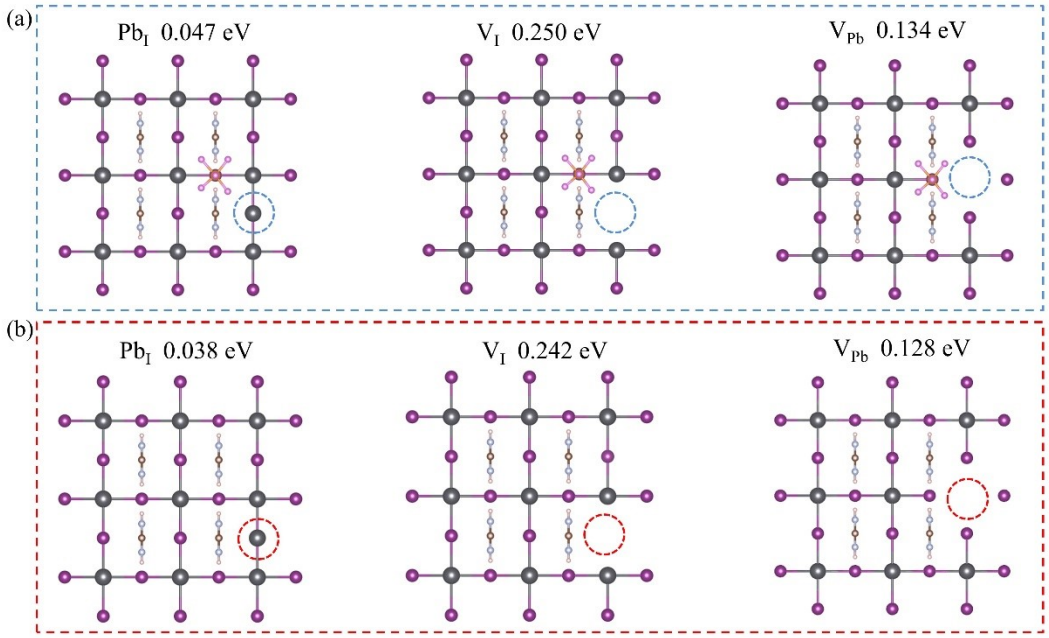

Fig. S9 Calculated structure illustration of the defect formation energies (a) after and (b) before PF_6^- adsorption on perovskite surfaces.

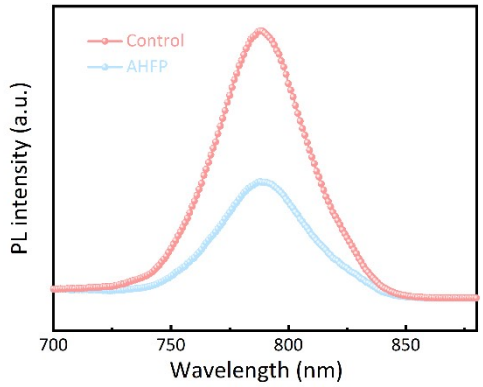

Fig. S10 Steady-state photoluminescence spectra of the perovskite films on the control or AHFP-treated SnO_2 ETL.

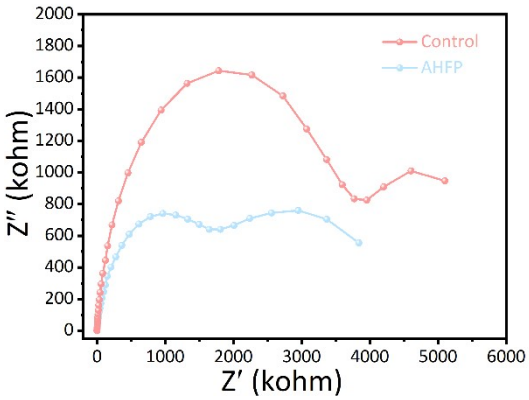

Fig. S11 Nyquist plots of devices the control or AHFP-treated SnO_2 ETL.

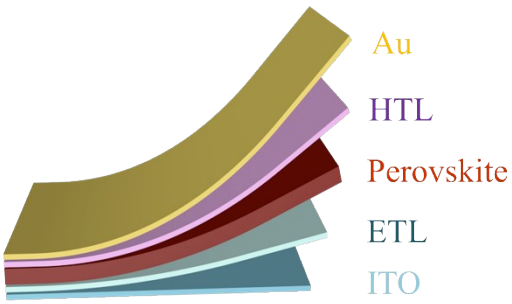

Fig. S12 Schematic diagram of the device structure.

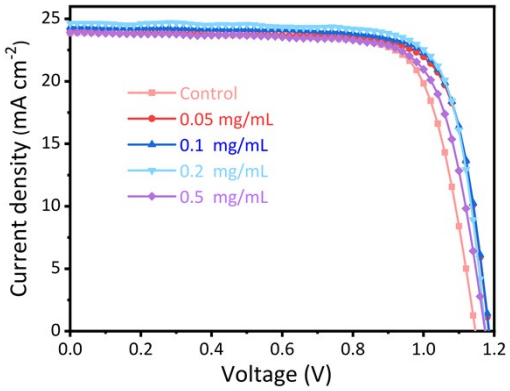

Fig. S13 *J*−*V* curves of devices with different concentrations of AHFP treatment.

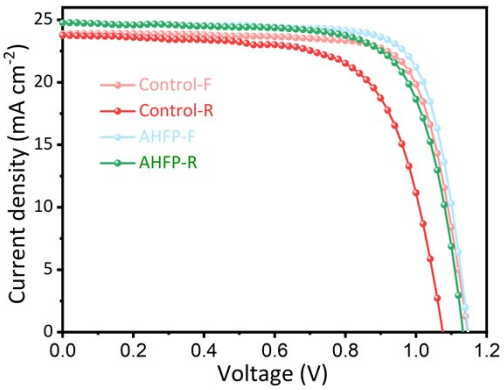

Fig. S14 *J*−*V* curves of devices with the control or AHFP-treated SnO_2 ETL under reverse and forward scan.

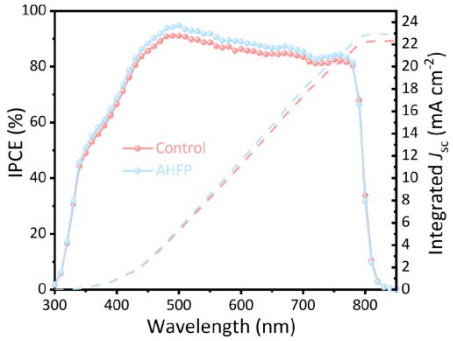

Fig. S15 IPCE spectra of the devices with control or AHFP-treated SnO_2 ETL.

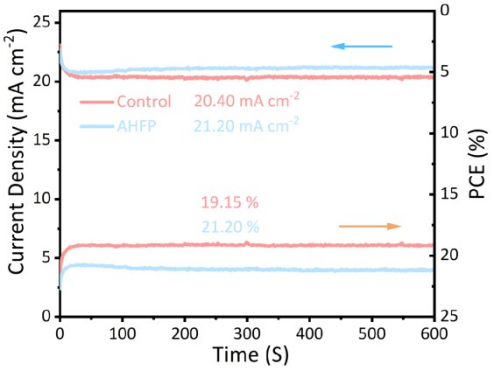

Fig. S16 Steady-state power output of the devices with control or AHFP-treated SnO_2 ETLs.

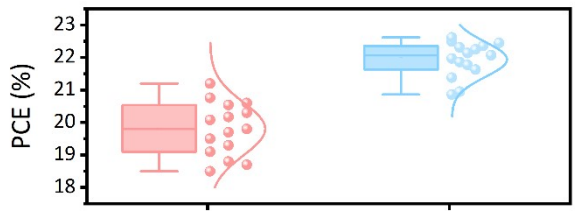

Fig. S17 Statistical optoelectronic parameters of PCE for devices with the control or AHFP-treated SnO_2 ETL.

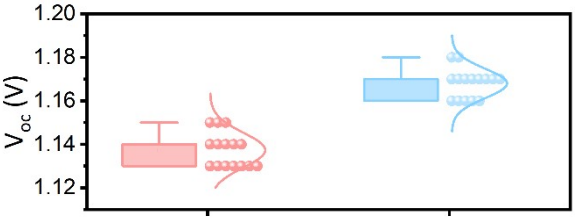

Fig. S18 Statistical optoelectronic parameters of V_{oc} for devices with the control or AHFP-treated SnO_2 ETL.

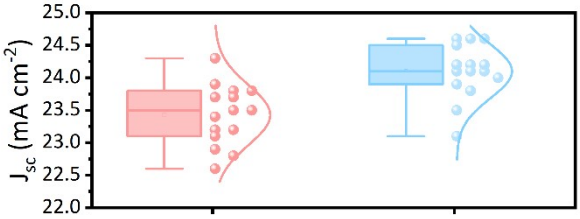

Fig. S19 Statistical optoelectronic parameters of J_{sc} for devices with the control or

AHFP-treated SnO_2 ETL.

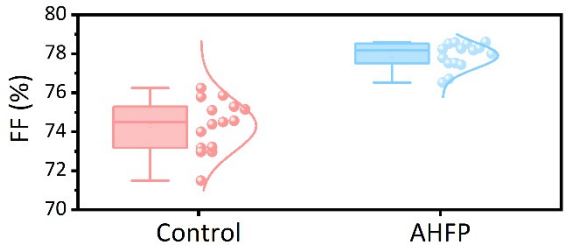

Fig. S20 Statistical optoelectronic parameters of FF for devices with the control or AHFP-treated SnO_2 ETL.

Table S1. Fitted results of EIS.

Sample	High frequency resistance(Ω)	Low frequency resistance(Ω)
Control	3.73×10^6	2.47×10^6
AHFP	1.62×10^6	2.67×10^6

Table S2. Photovoltaic parameters of the control and AHFP-modified devices in RS and FS under simulated AM 1.5G one sun illumination of 100 mW/cm^2.

Devices	J_{sc} (mA/cm^2)	V_{oc} (V)	FF (%)	PCE (%)
Control - Reverse	24.03	1.06	67.61	17.23
Control - Forward	24.08	1.15	75.92	20.98
HATP - Reverse	24.76	1.13	72.46	20.31
HATP - Forward	24.75	1.15	76.43	21.70

Reference

[1] Y. Zhang, T. Kong, H. Xie, J. Song, Y. Li, Y. Ai, Y. Han and D. Bi, *ACS Energy Lett*. 2022, **7**, 929-938.

[2] G. Liu, H. Zheng, J. Ye, S. Xu, L. Zhang, H. Xu, Z. Liang, X. Chen and Xu Pan, *ACS Energy Lett*. 2021, **6**, 4395-4404.

[3] R. Wang, J. Xue, K.-L. Wang, Z.-K. Wang, Y. Luo, D. Fenning, G. Xu, S. Nuryyeva, T. Huang, Y. Zhao, J. Lee Yang, J. Zhu, M. Wang, S. Tan, I. Yavuz, K. N. Houk and Y. Yang, *Science*, 2019, **366**, 1509-1513.